Applied Catalysis B: Environmental 209 (2017) 447–454

Contents lists available at ScienceDirect

Applied Catalysis B: Environmental

journal homepage: www.elsevier.com/locate/apcatb

2D nitrogen-doped hierarchically porous carbon: Key role of low dimensional structure in favoring electrocatalysis and mass transfer for oxygen reduction reaction

Kai Wan [a], Ai-dong Tan [a], Zhi-peng Yu [a], Zhen-xing Liang [a,*], Jin-hua Piao [b], Panagiotis Tsiakaras [c,d,**]

[a] Key Laboratory on Fuel Cell Technology of Guangdong Province, School of Chemistry and Chemical Engineering, South China University of Technology, Guangzhou 510641, PR China
[b] School of Food Science and Engineering, South China University of Technology, Guangzhou 510641, PR China
[c] Laboratory of Alternative Energy Conversion Systems, Department of Mechanical Engineering, School of Engineering, University of Thessaly, Pedion Areos, 38334 Volos, Greece
[d] Laboratory of Electrochemical Devices Based on Solid Oxide Proton Electrolytes, Institute of High Temperature Electrochemistry, Yekaterinburg 620990, Russia

ARTICLE INFO

Article history:
Received 28 November 2016
Received in revised form 10 February 2017
Accepted 1 March 2017
Available online 4 March 2017

Keywords:
Nitrogen-doped carbon
Ultrathin films
Hierarchically porous structure
Oxygen reduction reaction
Mass transfer

ABSTRACT

An ultrathin (thickness 1.0 nm) 2D nitrogen-doped hierarchically porous carbon (2DNHPC) film is developed by the nanocasting method; for comparison, a 3D nitrogen-doped ordered mesoporous carbon (3DNOMC) is also synthesized. Characterizations reveal that 2DNHPC is featured by an extremely high aspect ratio (several hundred) and a bimodal pore distribution. Such a 2D hierarchically porous structure is found to facilitate both the mass transfer of the reactive species and the utilization of active site in the electrode. First, 2DNHPC yields a larger limiting current than does 3DNOMC for the oxygen reduction reaction (ORR), revealing the key role of the low dimensional structure to facilitate the mass transfer. Second, at the loading of 500 μg cm^{-2}, 2DNHPC shows the same kinetic current with 3DNOMC, indicating that the two catalysts have the same active site and turnover frequency. In comparison, at a lower loading of 250 μg cm^{-2}, the kinetic current of 2DNHPC remains unchanged, which however seriously deteriorates for 3DNOMC. This result strongly highlights the effect of the carbon dimension on the utilization efficiency of the active site. Finally, it is noted that 2DNHPC yields a comparable ORR electrocatalytic activity and long-term stability with commercial Pt catalyst in both alkaline and acid media.

1. Introduction

Oxygen reduction reaction (ORR) is a key electrochemical process in both fuel cells [1] and metal-air batteries [2,3]. Platinum is acknowledged to be the best-performing catalyst; however, its source scarcity and high price seriously hinder the wide application of fuel cells [4,5]. Therefore, great efforts have been devoted to exploring alternative non-precious metal electrocatalysts with higher activity and lower cost [6–10].

Carbon has been regarded as one of the most promising Pt-alternative catalyst due to its low cost and tuneable properties [11–14]. Its electrocatalytic activity is determined by both the chemical nature and the density of the active sites. Following this philosophy, researchers have tried various strategies to increase the activity of the carbon catalyst. First, the precise control over the surface composition, like by nitrogen-doping, can effectively tune the chemical nature of the active site and thus increase the ORR turnover frequency [12,13,15]. The nitrogen doping can effectively activate the carbon atoms, which act as the active sites for the ORR [16–18]. Some researchers argue that the transition metal is also involved in the electrocatalysis of the ORR [6,19]. Second, a variety of nanostructured carbons are developed with inspiring features in terms of the electrochemical performance [20–23]. Dai [16] synthesized 1D nitrogen-doped carbon nanotubes by the chemical vapour

* Corresponding author. Key Laboratory on Fuel Cell Technology of Guangdong Province, School of Chemistry and Chemical Engineering, South China University of Technology, Guangzhou 510641, PR China
** Corresponding author at: Laboratory of Alternative Energy Conversion Systems, Department of Mechanical Engineering, School of Engineering, University of Thessaly, Pedion Areos, 38334 Volos, Greece.
E-mail addresses: zliang@scut.edu.cn (Z.-x. Liang), tsiak@uth.gr, tsiak@mie.uth.gr (P. Tsiakaras).

http://dx.doi.org/10.1016/j.apcatb.2017.03.014
0926-3373/

deposition method, which features a facile charge transfer and thus a high activity. 2D graphene has an extremely high specific surface area (2620 $m^2 g^{-1}$), which is supposed to favour the exposure of the active sites in catalysis. Feng [24] synthesized 2D graphene-based carbon nitride nanosheets for the ORR; however, the advantage is not remarkable in practice due to the serious aggregation of the carbon sheets [25]. Nitrogen ordered mesoporous carbon features a high and accessible specific surface area, which thereby favours the catalysis [15,26,27].

As known, apart from the catalysis itself, the mass transfer is of great importance in terms of the concentration polarization and the utilization efficiency of the active sites [28–30]. Therefore, the rational design of the electrocatalyst closely relies on the understanding of the electrode processes besides the structural motif of the material. For example, hierarchically porous carbon can indeed facilitate the mass transfer and has recently attracted considerable attention [31–41]. Lu [36] developed 3D nitrogen-doped hierarchically porous carbon, which enables a low mass transfer resistance and improve the accessibility of catalytic sites. Qiao [37] developed nitrogen-doped ordered macro-mesoporous carbon/graphene *via* a dual-template method. Such a hierarchically porous structure facilitates the mass transport in the catalyst layer and thus enhances the electrocatalytic activity to the ORR.

In a previous work, we synthesized 3D nitrogen-doped ordered mesoporous carbon (3DNOMC), which showed a high specific surface area, uniform pore structure and decent electrocatalytic activity [15,42–44]. The superior activity indicates that active sites *viz.* nitrogen-activated carbon atoms, are densely assembled in the carbon catalyst. However, the limiting current density is much lower than that of the Pt/C catalyst [15]. The inferior behaviour indicates that most active sites, which are anchored on the surface of the deep long-range mesopores, are inaccessible to the reactive species, like oxygen. To lower the dimension of the material is supposed to be effective in addressing this concentration polarization loss and improve the utilization efficiency of the active sites.

In the present work, we developed an ultrathin 2D nitrogen-doped hierarchically porous carbon (2DNHPC), which features a high specific surface area (594 $m^2 g^{-1}$), nanoscale dimension in thickness (1.0 nm), and hierarchically meso/macroporous structure. The above features enable both the easy mass transfer and high utilization efficiency of the densely-assembled active sites. In line with this rational design, 2DNHPC is highly effective in catalysing the ORR in both acid and alkaline media. For comparison reasons, 3DNOMC is synthesized with a similar surface area and the same active sites. It is found that 2DNHPC exhibits a superior performance to the latter one, especially at a low catalyst loading, highlighting the importance of the mass transfer and utilization efficiency of the active sites.

2. Experimental

2.1. Material preparation

2.1.1. Synthesis of the silica templates

2.1.1.1. SBA-15. The synthesis of SBA-15 was described in details elsewhere [45]. Typically, 4.0 g tri-block copolymer $EO_{20}PO_{70}EO_{20}$ (Pluronic P123, BASF) was dissolved in 126 mL deionized (DI) water and 20 mL HCl (AR, 37 wt%, Sinopharm Chemical Reagent Co., Ltd) solution. Then, 9.2 mL tetraethylorthosilicate (AR, TEOS, Sinopharm Chemical Reagent Co., Ltd) was added and stirred for 20 h at 35 °C. The slurry was hydrothermally treated at 100 °C for 24 h. Finally, the powders were collected and subjected to a microwave-digestion to remove the organic template [46].

2.2. 2D hierarchically porous silica film (2DHPS)

The same protocol was used to synthesize a 2D hierarchically porous silica film except that graphene oxide (GO, Ningbo Institute of Material Technology and Engineering) was added as a co-template [47]. GO was dissolved in the aqueous mixture containing P123 and HCl, of which the concentration was 4.23 mg mL^{-1}.

2.2.1. Synthesis of nitrogen-doped carbon

Nitrogen-doped carbon was synthesized by a nanocasting method. First, 3.0 g 1,10-phenanthroline monohydrate ($C_{12}H_8N_2{\cdot}H_2O$, AR, Xiya Reagent) was dissolved in a mixture of 30.0 mL ethanol and 30.0 mL $FeCl_2$ (AR, Sinopharm Chemical Reagent Co., Ltd) solution. The molar ratio of iron to phenanthroline was 1:3, ensuring that the phenanthroline was completely coordinated with the ferrous ion. Second, a certain amount of silica template (SBA-15: 3.27 g, 2DHPS: 2.75 g) was dispersed in the solution and sonicated for 6 h at room temperature. Third, after the solvent was evaporated, the obtained powders were pyrolyzed at 900 °C (heating rate: 15 °C min^{-1}, MTI, Hefei, China) for 3 h in argon (99.999%). Finally, the nitrogen-doped carbon material was obtained after a two-step chemical leaching: i) to remove the silicate template by boiling in 10 M NaOH (AR, Sinopharm Chemical Reagent Co., Ltd) at 120 °C for 24 h; and ii) to remove the dissolvable iron species by boiling in 0.10 M $HClO_4$ (AR, Sinopharm Chemical Reagent Co., Ltd) at 80 °C for 24 h.

The nitrogen-doped carbon materials were referred to as 2D nitrogen-doped hierarchically porous carbon (2DNHPC) and 3D nitrogen-doped ordered mesoporous carbon (3DNOMC), which were respectively derived from 2DHPS and SBA-15 as the silica template.

2.3. Physical characterizations

Transmission electron microscopy (TEM) was performed on a FEI Tecnai G2 F20 S-TWIN operated at 200 kV. Tapping mode atomic force microscope (AFM) experiment was performed on Bruker Multimode 8. X-ray photoelectron spectroscopy (XPS, Physical Electronics PHI 5600, US) measurement was carried out with a multi-technique system using an Al monochromatic X-ray at a power of 350 W. The pore structures of samples were probed by nitrogen adsorption/desorption isotherms at 77 K (Micromeritics ASAP 2020, US). Before each measurement, the samples were outgassed at 200 °C for 12 h. The specific surface area was determined by Brunauer-Emmett-Teller (BET) model, while the pore size and volume were calculated by the density functional theory (DFT) method on the built-in software.

2.4. Electrochemical characterization

The electrochemical behaviour of the carbon material was characterized by the cyclic voltammetry (CV) and linear sweeping voltammetry (LSV) using a three electrode cell with an electrochemical work station Zennium (Zahner) at room temperature (25 °C). A gold wire and a double junction Ag/AgCl reference electrode (PINE) were used as the counter and reference electrodes, respectively. The working electrode was a rotating disk electrode (Glassy carbon disk: 5.0 mm in diameter, RDE). The thin-film electrode on the disk was prepared as follows. 10 mg of the catalyst was dispersed in 1.0 mL Nafion/ethanol (0.84 wt% Nafion) by sonication for 60 min. Then, 10 μL of the dispersion was transferred onto the glassy carbon disk by using a pipette, yielding the catalyst loading of 0.50 mg cm^{-2}. For comparison reasons, the electrocatalytic activity for ORR of the commercial 40 wt% Pt/C catalyst (HiSPEC4000, Johnson Matthey) was also evaluated with the metal loading of 20 μg cm^{-2}.

For the CV tests, the electrolyte solution (0.10 M KOH and 0.10 M $HClO_4$) was first bubbled with argon for 60 min. The cyclic voltammograms were recorded at 20 mV s^{-1} in the potential range between 0 and 1.23 V (*vs.* reversible hydrogen electrode, RHE) for 20 cycles.

If unspecified, linear sweeping voltammograms were recorded by scanning the disk potential from 1.23 down to 0 V at a rate of 5 mV s^{-1} in oxygen-saturated electrolyte solution under 1600 rpm, from which the ORR polarization curve was extracted by subtracting the capacitive current.

The stability of the catalysts were evaluated by collecting the chronoamperometric curve at 0.90 V(*vs.* RHE) in O_2-saturated 0.10 M KOH solution, and 0.80 V in O_2-saturated 0.10 M $HClO_4$ solution. Also, an accelerated protocol was also employed for the evaluation by cycling the potential between 0.6 and 1.0 V for 5000 cycles. During the potential cycling, the polarization curve was at intervals collected to track the degradation of the catalysts.

3. Results and discussion

Fig. 1 depicts the TEM images of the 2D hierarchically porous silica (2DHPS) film and the 2D nitrogen-doped hierarchically porous carbon (2DNHPC) film. Figs. 1a-b reveal that silica is thin film associated with parallel mesochannels, of which the diameter is uniform at *ca.* 5 nm. The formation of the 2D mesoporous film can be understood as follows. First, the parallel mesochannels originate from the template – the P123 micelles, as well acknowledged in the synthesis of SBA-15 (see Fig. S1a-b) [15,42,43]. Second, the 2D morphology results from the co-template GO (graphene oxide), on which the silica precursor experiences the co-operative assembly [47].

In comparison, in absence of GO, SBA-15 is 3D interconnected short bars (see Fig. S1a-b). It is well acknowledged that in the nanocasting method, the resultant carbon inherits the inverse replica of the hard template. In line with this understanding, the resultant carbon is found to be a thin film with built-in mesopores (see Fig. 1c-d), while 3DNOMC is bar-like block (see Fig. S1c-d).

Atomic force microscope (AFM) was employed to measure the morphological features of the film. Fig. 2a-b suggest that the silica and resultant carbon have similar characteristic size, and the thickness is respective to be 4.0 and 1.0 nm.

The aspect ratio of the two materials is extremely high up to several hundred, which confirms the above analysis that both silica and carbon are 2D film. In addition, the surface of 2DNHPC is less complete than that of the template 2DHPS, and considerable larger pores with the diameter of 30–100 nm are observed in the carbon film (circle-noted, see Fig. 2c). These larger pores are generated due to the decomposition of the carbon precursor and the consequent evolution of gas bubbles during the pyrolysis.

Fig. 3 shows the nitrogen ad/desorption isotherms of the silica template and corresponding carbon. As it can be seen in Fig. 3a, SBA-15 exhibits a typical type-IV isotherm with an H1 hysteresis loop, which is indicative of a narrow range of uniform mesopores. 2DHPS also shows a type-IV isotherm, which is however associated with a unique hysteresis loop with H3 and H5 features [48]. It is, thus, inferred that 2DHPS is a hierarchically porous silica template, which contains both mesopores (open and partially-blocked) and macropores (see Fig. S2a) [41,43,48]. Fig. 3b shows the isotherms of the resultant carbon materials. Inheriting from the template, the resultant carbon also shows a type-IV isotherm with an H3 hysteresis loop, indicating their hierarchically porous structure. The

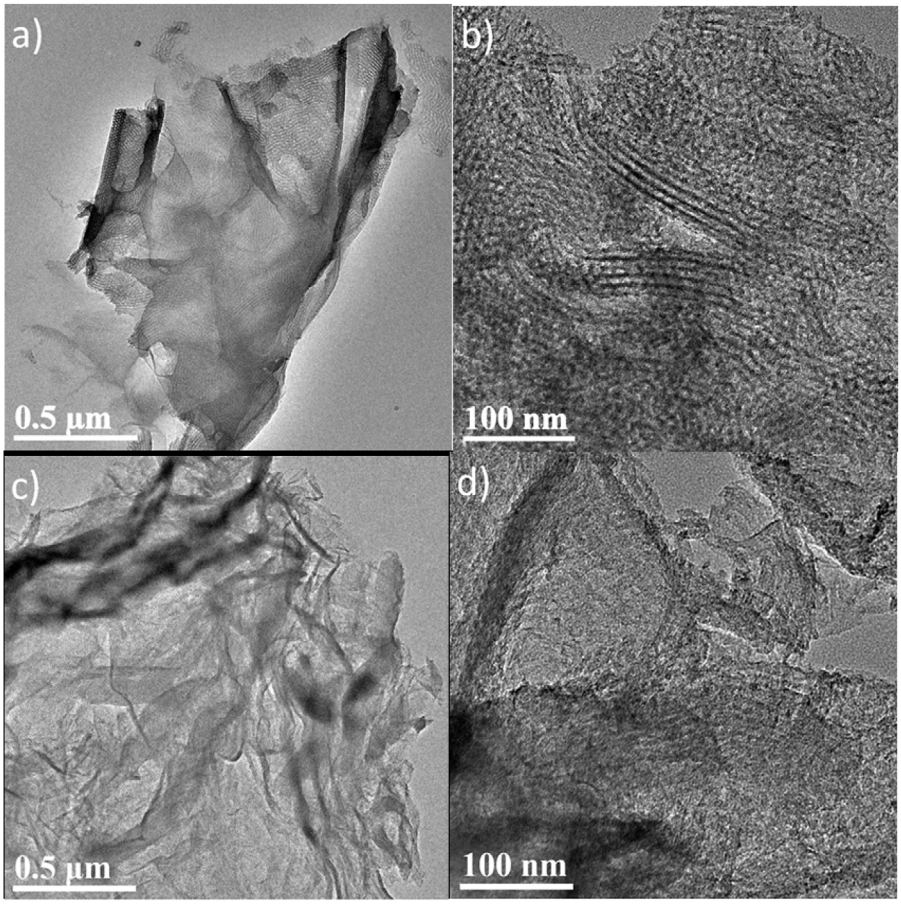

Fig. 1. TEM images: a-b) 2D hierarchically porous silica film; c-d) 2D nitrogen-doped hierarchically porous carbon film.

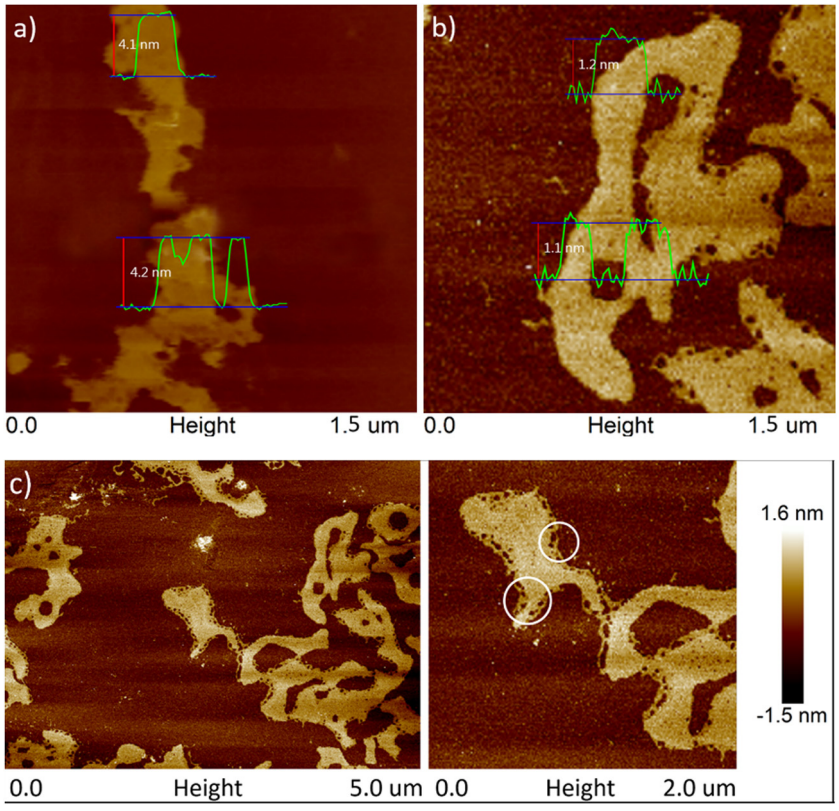

Fig. 2. AFM images: a) 2D hierarchically porous silica film; b-c) 2D nitrogen-doped hierarchically porous carbon film.

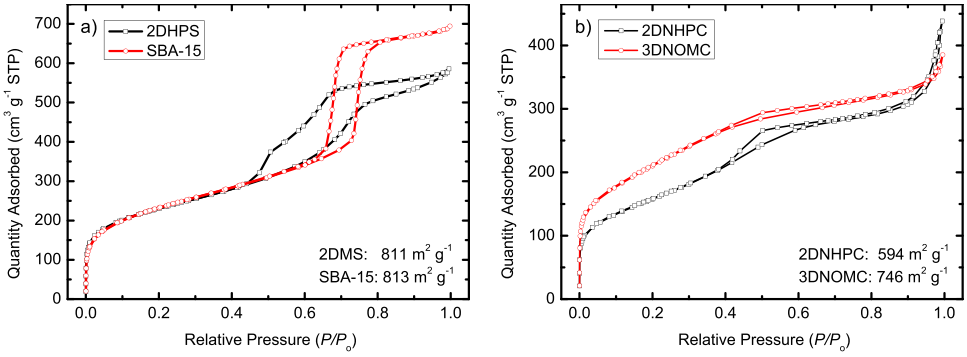

Fig. 3. Nitrogen sorption isotherms of the silica template a), and the resultant carbon b).

presence of secondary porosity of macropores (see Fig. S2b) on the surface of 2DNHPC is also seen in the above AFM images.

Its pore diameter is centred at *ca.* 4.0, 16.0 and 35 nm, and the pore volume is 0.68 $cm^3\ g^{-1}$. These pore features enable the sufficient exposure and accessibility of the ORR active sites. The specific surface area (A_{BET}) of 2DNHPC is found to be 594 $m^2\ g^{-1}$, which is much higher than the conventional 2D graphene. This feature endows 2DNHPC, as either the catalyst itself or the support for Pt, with a superior electrochemical performance of the ORR, as shown below.

In comparison, 3DNOMC exhibits a much larger specific surface area of 746 $m^2\ g^{-1}$, which is seemingly more effective than 2DNHPC in electrocatalysis. However, it is noted that the higher specific surface area is mainly contributed by the long-range bulky mesopores in 3DNOMC. This morphological feature raises the concern on the utilization efficiency of the active sites. The active sites in the 'deep' mesopores are probably inaccessible to the active species (like dissolved oxygen, protons) at a higher current density, which, therefore, cannot be fully utilized in electrocatalysis (*vide infra*).

Table 1
Elemental composition (at.%) of the resultant carbon materials measured by XPS.

Sample	C	N	O	Fe	N:C
2DNHPC	85.22	3.29	11.21	0.21	0.039
3DNOMC	89.65	3.33	6.50	0.34	0.037

XPS was employed to characterize the surface composition (see Fig. S3). The elemental content is listed in Table 1. The two carbon materials show the same nitrogen content of 3.3 at.% (3.29 at.% for 2DNHPC and 3.33 at.% for 3DNOMC). This result is understandable as the two templates have similar porous structure, and thereby, yield negligible difference in the spacial nanoconfinement effect [49]. It is inferred that the chemical configuration of carbon and dopant nitrogen should be similar. In Fig. 4 the high-resolution spectra of N 1s and C 1s is depicted.

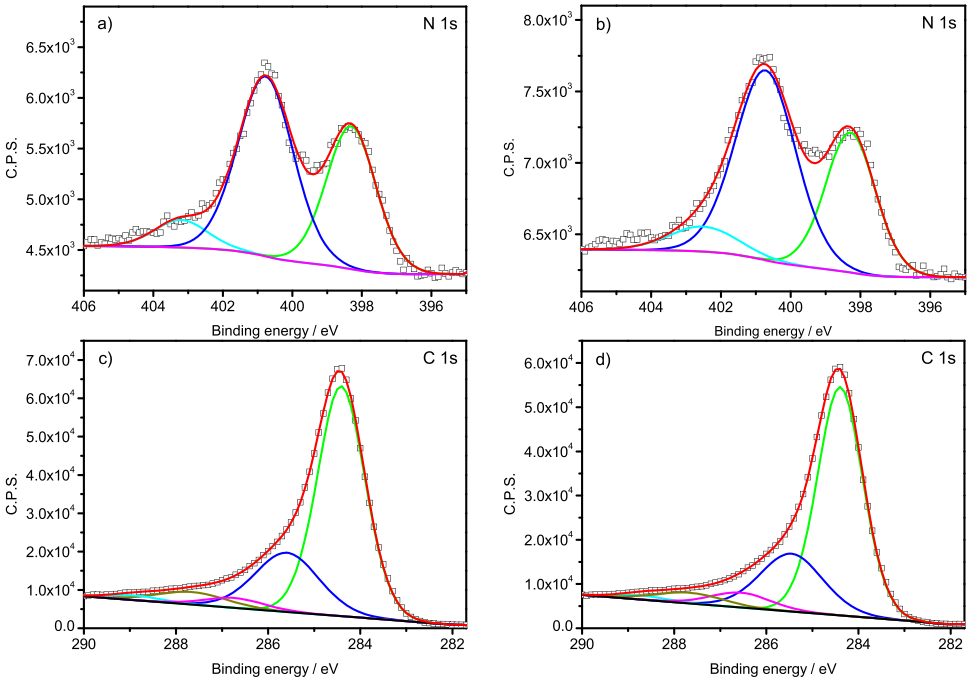

Fig. 4. N 1s peak of 2DNHPC (a) and 3DNOMC (b); C 1s peak of 2DNHPC (c) and 3DNOMC (d).

To quantify the configuration, the N 1s (see Fig. 4a-b, Table S1) is deconvoluted to three peaks with binding energy at 398.4 ± 0.2, 401.0 ± 0.1 and 401.5–404 eV, which respectively correspond to pyridinic-, graphitic-, and oxide-nitrogen [50,51]. It is seen that the content of each nitrogen component is similar for the two carbons, confirming the above analysis. Similarly, the fitting results of the C 1s spectra (see Fig. 4c-d, Table S2) lead to the same conclusion. The nitrogen-activated carbon, which is claimed to be the active site for the ORR [15,27], shows the same content (*ca.* 23%) in the two carbon samples. As such, the two carbons, used as the ORR electrocatalysts, should have the same intrinsic electrocatalytic activity (*vide infra*).

Fig. 5 shows the cyclic voltammograms of the two carbons in either 0.10 M KOH or 0.10 M $HClO_4$ solution. It is seen that the electrochemical features are similar for the two carbons in the two electrolyte solutions. A pair of broad symmetrical redox peaks are found in the potential range of 0–0.9 V in alkaline media and 0.4–0.9 V in acid media, indicating a variety of enriched electrochemically active functional groups on the carbon surface.

These electrochemical transitions have been acknowledged to originate from the reversible redox couples like hydroquinone-/quinone-like groups [52]. In comparison with 3DNOMC, 2DNHPC shows a smaller capacitive current, which may be attributed to its lower specific surface area (*vide supra*).

Fig. 6 shows the ORR polarization curves of the nitrogen-doped carbon and commercial Pt/C catalyst. From Fig. 6a, the onset potential is found to be 0.900 V for Pt/C and 0.945 V for two carbon catalysts. This result suggests that the two catalysts exhibit a much better ORR electrocatalytic activity than does the Pt/C catalyst in alkaline media. In addition, it is seen that the polarization curves of the carbon catalysts are well overlapped at potentials above 0.85 V, indicating their same electrocatalytic activity. The result is unsurprising as the content of the active sites is same for the two catalysts, as discussed in XPS section. With further decreasing the potential (0-0.8 V), a notable deviation in the two curves is observed.

The limiting current is found to be close to 6 mA cm^{-2} for 2DNHPC, which is higher than that measured on 3DNOMC (5 mA cm^{-2}). This finding is strongly indicative of the more facile mass transfer of oxygen into the 2D hierarchically porous carbon catalyst, which thereby yields a higher utilization efficiency of the active sites. The same trend is also seen in acid media (see Fig. 6b). The effect of the utilization efficiency of the active site is further manifested by decreasing the catalyst loading, as shown below.

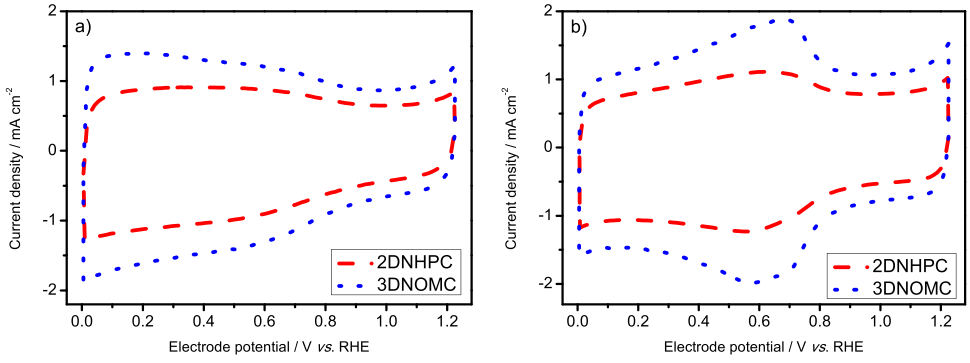

Fig. 5. Cyclic voltammograms of 2DNHPC and 3DNOMC in: a) Ar-saturated 0.10 M KOH solution; b) Ar-saturated 0.10 M $HClO_4$ solution.

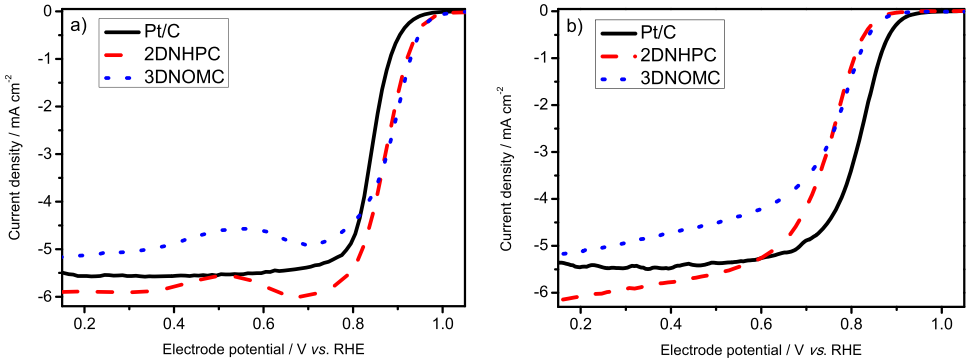

Fig. 6. The ORR polarization curves of 2DNHPC and 3DNOMC: a) O_2-saturated 0.10 M KOH; b) O_2-saturated 0.10 M $HClO_4$.

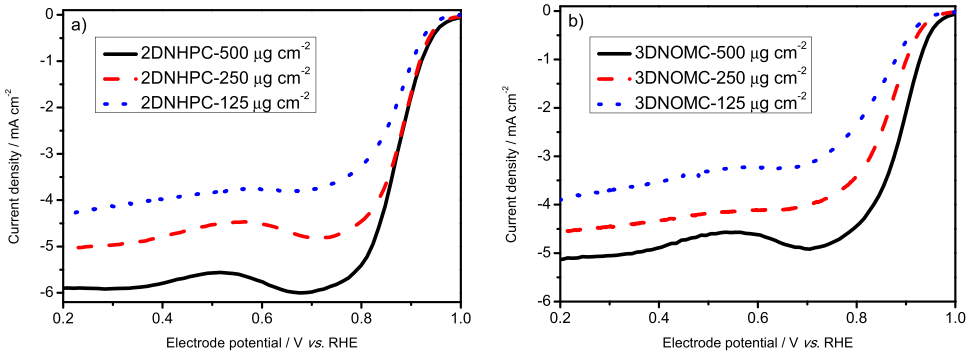

Fig. 7. The ORR polarization curves of 2DNHPC (a) and 3DNOMC (b) with three different loadings in the O_2-saturated 0.10 M KOH.

It is well acknowledged that the loading of the catalyst is of paramount importance to the ORR kinetics. The decrease in the loading seriously deteriorates the kinetic current of the carbon catalysts, as it can be seen from Fig. 7; more obviously for 3DNOMC than for 2DNHPC. At potentials above 0.85 V, the kinetic current density basically remains unchanged for 2DNHPC when the loading decreases from 500 to 250 $\mu g\,cm^{-2}$; in comparison, for 3DNOMC the current density at 0.85 V decreases from 3.73 to 2.49 $mA\,cm^{-2}$.

Such a difference in the two carbon catalysts can be attributed to the utilization efficiency of the active site on the carbon surface. It is stated in the physical ad/desorption section, that the surface of 2DNHPC is more accessible to the reactive species in the ORR than 3DNOMC, which yields a much higher utilization efficiency of the active sites. It is understandable that at a high catalyst loading, the amount of active sites is sufficient to yield a high kinetic current; however, as the loading decreases, the active sites gets fewer and the utilization efficiency plays a more pronounced role in determining the kinetics. 2DNHPC features a high utilization efficiency of the active site and is thus not that sensitive to the loading as 3DNOMC. The same trend is also observed in acid media (see Fig. S4). Finally, it is inspiring to note that the 2DNHPC catalyst yields a comparable electrocatalytic activity to the Pt/C catalyst in both acid and alkaline media, which is of particular interests for fuel cell applications.

In addition, the stability of the catalysts was studied by collecting the chronoamperometric curve (i–t), as shown in Fig. 8. Fig. 8a shows that in alkaline media, Pt/C catalyst yields 72% drop in current after 25-h continuous operation. In comparison, the two carbon catalysts show a much smaller decay of 18%. The trend is similar in acid media. The current drops to 10% for Pt/C, 70% for 3DNOMC, and 72% for 2DNHPC. The above results reveal that the nitrogen-doped carbon catalysts have a much higher stability than does the commercial Pt/C catalyst in both acid and alkaline media. The accelerated degradation result (see Fig. S5) confirms these findings. During the potential cycling, the degradation in the electrochemical performance is much less for 2DNHPC than the Pt/C catalyst.

The superior stability of the carbon catalyst may lie in the high electrochemical reversibility of the active site. In our previous work, the carbon-containing functional groups have been suggested to the active site for the ORR, which are highly electrochemically reversible in both acidic and alkaline media [18]. That means, the oxidized species on the surface can be easily generated and stripped off in mediating the ORR. As the evidence, the hysteresis loop is not found in collecting the cyclic polarization curves of the ORR [18]. In comparison, the Pt/C catalyst shows a broad hysteresis loop, indicating that oxidized Pt is not that electrochemically active to get reduced. This inevitably leads to the dissolution/redeposition and the consequent degradation of the Pt/C catalyst.

4. Conclusions

An ultrathin 2D nitrogen-doped hierarchically porous carbon (2DNHPC) film was developed in this work.

Extensive characterizations revealed that the 2DNHPC film featured an ultrathin thickness (1.0 nm), an extremely high aspect ratio (several hundred) and a hierarchically porous structure containing both mesopores and macropores. This unique 2D hierarchically porous structure was found to favour both the mass transfer of the reactive species and the utilization of active site, promoting the oxygen reduction reaction (ORR). First, 2DNHPC yielded a larger limiting current density than did a 3D nitrogen-doped mesoporous carbon (3DNOMC), revealing the key role of the low dimension to facilitate the mass transfer. Second, when the catalyst loading decreased, the kinetic current for 2DNHPC remained unchanged, but seriously deteriorated for 3DNOMC, indicating a high utilization efficiency of the active site in 2DNHPC.

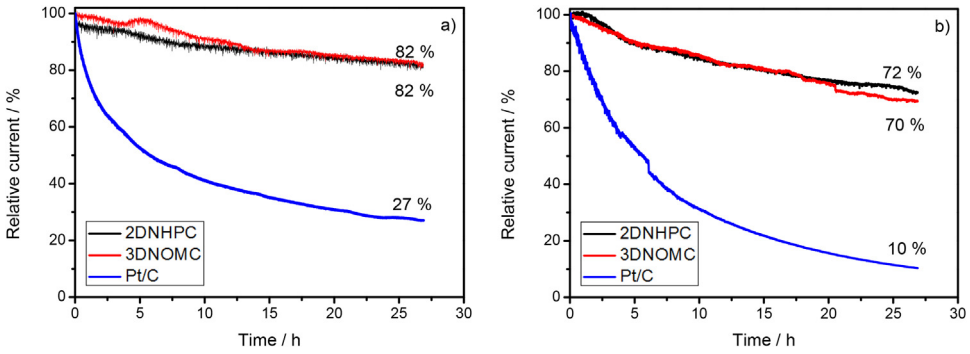

Fig. 8. The chronoamperometric curves of the three catalysts: a) at 0.90 V (*vs.* RHE) in the O_2-saturated 0.10 M KOH, b) at 0.80 V (*vs.* RHE) in the O_2-saturated 0.10 M $HClO_4$.

The above findings strongly highlight the key role of the dimension of carbon in electrocatalysis. Finally, it is noted that 2DNHPC yielded a comparable ORR electrocatalytic activity and superior stability to the commercial Pt catalyst in both alkaline and acid media.

This work does not only provide a high-performance carbon catalyst for the ORR, but also shed light on the importance of the dimension of the material in terms of the mass transfer and utilization efficiency of the active sites.

Acknowledgements

The work described in this paper was jointly supported by the National Natural Science Foundation of China (Nos. 21476087, 21576101, 21676106), National Key Research and Development Program of China (No. 2016YFB0101200 (2016YFB0101204)), and the Fundamental Research Funds for the Central Universities. Prof. Tsiakaras is also grateful to the "Bilateral R&D Cooperation program between Greece-China 2012–2014" and the Ministry of Education and Science of the Russian Federation (Mega-Grant, contract no. 14.Z50.31.0001) for funding.

Appendix A. Supplementary data

Supplementary data associated with this article can be found, in the online version, at http://dx.doi.org/10.1016/j.apcatb.2017.03.014.

References

[1] M.K. Debe, Electrocatalyst approaches and challenges for automotive fuel cells, Nature 486 (2012) 43–51.
[2] P. Zhang, F. Sun, Z.H. Xiang, Z.G. Shen, J. Yun, D.P. Cao, ZIF-derived in situ nitrogen-doped porous carbons as efficient metal-free electrocatalysts for oxygen reduction reaction, Energy Environ. Sci. 7 (2014) 442–450.
[3] C. Liao, Q. Xu, C. Wu, D. Fang, S. Chen, S. Chen, J. Luo, L. Li, Core-shell nano-structured carbon composites based on tannic acid for lithium-ion batteries, J. Mater. Chem. A 4 (2016) 17215–17224.
[4] G. Wu, P. Zelenay, Nanostructured nonprecious metal catalysts for oxygen reduction reaction, Acc. Chem. Res. 46 (2013) 1878–1889.
[5] G.F. Long, X.H. Li, K. Wan, Z.X. Liang, J.H. Piao, P. Tsiakaras, Pt/CN-doped electrocatalysts: Superior electrocatalytic activity for methanol oxidation reaction and mechanistic insight into interfacial enhancement, Appl. Catal. B: Environ. 203 (2017) 541–548.
[6] G. Wu, K.L. More, C.M. Johnston, P. Zelenay, High-performance electrocatalysts for oxygen reduction derived from polyaniline, iron, and cobalt, Science 332 (2011) 443–447.
[7] Y. Hua, T. Jiang, K. Wang, M. Wu, S. Song, Y. Wang, P. Tsiakaras, Efficient Pt-free electrocatalyst for oxygen reduction reaction: highly ordered mesoporous N and S co-doped carbon with saccharin as single-source molecular precursor, Appl. Catal. B: Environ. 194 (2016) 202–208.
[8] T. Jiang, Y. Wang, K. Wang, Y. Liang, D. Wu, P. Tsiakaras, S. Song, A novel sulfur-nitrogen dual doped ordered mesoporous carbon electrocatalyst for efficient oxygen reduction reaction, Appl. Catal. B: Environ. 189 (2016) 1–11.
[9] X.H. Li, K. Wan, Q.B. Liu, J.H. Piao, Y.Y. Zheng, Z.X. Liang, Nitrogen-doped ordered mesoporous carbon: Effect of carbon precursor on oxygen reduction reactions, Chin. J. Catal. 37 (2016) 1562–1568.
[10] H. Tang, Y. Zeng, D. Liu, D. Qu, J. Luo, K. Binnemans, D.E.D. Vos, J. Fransaer, D. Qu, S.G. Sun, Dual-doped mesoporous carbon synthesized by a novel nanocasting method with superior catalytic activity for oxygen reduction, Nano Energy 26 (2016) 131–138.
[11] L.M. Rivera Gavidia, G. García, D. Anaya, A. Querejeta, F. Alcaide, E. Pastor, Carbon-supported Pt-free catalysts with high specificity and activity toward the oxygen reduction reaction in acidic medium, Appl. Catal. B: Environ. 184 (2016) 12–19.
[12] T. Sun, L. Xu, S. Li, W. Chai, Y. Huang, Y. Yan, J. Chen, Cobalt-nitrogen-doped ordered macro-/mesoporous carbon for highly efficient oxygen reduction reaction, Appl. Catal. B: Environ. 193 (2016) 1–8.
[13] E. Bayram, G. Yilmaz, S. Mukerjee, A solution-based procedure for synthesis of nitrogen doped graphene as an efficient electrocatalyst for oxygen reduction reactions in acidic and alkaline electrolytes, Appl. Catal. B: Environ. 192 (2016) 26–34.
[14] X. Su, J. Liu, Y. Yao, Y. You, X. Zhang, C. Zhao, H. Wan, Y. Zhou, Z. Zou, Solid phase polymerization of phenylenediamine toward a self-supported FeN(x)/C catalyst with high oxygen reduction activity, Chem. Commun. 51 (2015) 16707–16709.
[15] K. Wan, G.F. Long, M.Y. Liu, L. Du, Z.X. Liang, P. Tsiakaras, Nitrogen-doped ordered mesoporous carbon: synthesis and active sites for electrocatalysis of oxygen reduction reaction, Appl. Catal. B: Environ. 165 (2015) 566–571.
[16] K. Gong, F. Du, Z. Xia, M. Durstock, L. Dai, Nitrogen-doped carbon nanotube arrays with high electrocatalytic activity for oxygen reduction, Science 323 (2009) 760–764.
[17] D.H. Guo, R. Shibuya, C. Akiba, S. Saji, T. Kondo, J. Nakamura, Active sites of nitrogen-doped carbon materials for oxygen reduction reaction clarified using model catalysts, Science 351 (2016) 361–365.
[18] K. Wan, Z.P. Yu, X.H. Li, M.Y. Liu, G. Yang, J.H. Piao, Z.X. Liang, pHeffect on electrochemistry of nitrogen-doped carbon catalyst for oxygen reduction reaction, ACS Catal. 5 (2015) 4325–4332.
[19] M. Lefevre, E. Proietti, F. Jaouen, J.P. Dodelet, Iron-based catalysts with improved oxygen reduction activity in polymer electrolyte fuel cells, Science 324 (2009) 71–74.
[20] C. Domínguez, F.J. Pérez-Alonso, M. Abdel Salam, S.A. Al-Thabaiti, A.Y. Obaid, A.A. Alshehri, J.L. Gómez de la Fuente, J.L.G. Fierro, S. Rojas, On the relationship between N content, textural properties and catalytic performance for the oxygen reduction reaction of N/CNT, Appl. Catal. B: Environ. 162 (2015) 420–429.
[21] Y.F. Song, J. Yang, K. Wang, S. Haller, Y.G. Wang, C.X. Wang, Y.Y. Xia, In-situ synthesis of graphene/nitrogen-doped ordered mesoporous carbon nanosheet for supercapacitor application, Carbon 96 (2016) 955–964.
[22] L. Zhou, P. Fu, D. Wen, Y. Yuan, S. Zhou, Self-constructed carbon nanoparticles-coated porous biocarbon from plant moss as advanced oxygen reduction catalysts, Appl. Catal. B: Environ. 181 (2016) 635–643.
[23] C.H. Choi, M.W. Chung, H.C. Kwon, J.H. Chung, S.I. Woo, Nitrogen-doped graphene/carbon nanotube self-assembly for efficient oxygen reduction reaction in acid media, Appl. Catal. B: Environ. 144 (2014) 760–766.
[24] S. Yang, X. Feng, X. Wang, K. Müllen, Graphene-based carbon nitride nanosheets as efficient metal-free electrocatalysts for oxygen reduction reactions, Angew. Chem. Int. Ed. 50 (2011) 5339–5343.
[25] B. Mendoza-Sánchez, Y. Gogotsi, Synthesis of two-dimensional materials for capacitive energy storage, Adv. Mater. 28 (29) (2016) 6104–6135.
[26] T. Lin, I.-W. Chen, F. Liu, C. Yang, H. Bi, F. Xu, F. Huang, Nitrogen-doped mesoporous carbon of extraordinary capacitance for electrochemical energy storage, Science 350 (2015) 1508–1513.
[27] M. Wu, J. Wang, Z. Wu, H.L. Xin, D. Wang, Synergistic enhancement of nitrogen and sulfur co-doped graphene with carbon nanosphere insertion for the electrocatalytic oxygen reduction reaction, J. Mater. Chem. A 3 (2015) 7727–7731.

[28] X.J. Zhou, Z.Y. Bai, M.J. Wu, J.L. Qiao, Z.W. Chen, 3-Dimensional porous N-doped graphene foam as a non-precious catalyst for the oxygen reduction reaction, J. Mater. Chem. A 3 (2015) 3343–3350.
[29] J. Wei, Y.X. Hu, Y. Liang, B.A. Kong, J. Zhang, J.C. Song, Q.L. Bao, G.P. Simon, S.P. Jiang, H.T. Wang, Nitrogen-doped nanoporous carbon/graphene nano-sandwiches: synthesis and application for efficient oxygen reduction, Adv. Funct. Mater. 25 (2015) 5768–5777.
[30] R. Li, Z.D. Wei, X.L. Gou, Nitrogen and phosphorus dual-doped graphene/carbon nanosheets as bifunctional electrocatalysts for oxygen reduction and evolution, ACS Catal. 5 (2015) 4133–4142.
[31] K.W. Tan, B. Jung, J.G. Werner, E.R. Rhoades, M.O. Thompson, U. Wiesner, Transient laser heating induced hierarchical porous structures from block copolymer-directed self-assembly, Science 349 (2015) 54–58.
[32] H.W. Liang, X. Zhuang, S. Bruller, X. Feng, K. Mullen, Hierarchically porous carbons with optimized nitrogen doping as highly active electrocatalysts for oxygen reduction, Nat. Commun. 5 (2014) 4973.
[33] Z.Y. Guo, C.C. Jiang, C. Teng, G.Y. Ren, Y. Zhu, L. Jiang, Sulfur, trace nitrogen and iron codoped hierarchically porous carbon foams as synergistic catalysts for oxygen reduction reaction, ACS Appl. Mater. Interfaces 6 (2014) 21454–21460.
[34] R. Balgis, T. Ogi, A.F. Arif, G.M. Anilkumar, T. Mori, K. Okuyama, Morphology control of hierarchical porous carbon particles from phenolic resin and polystyrene latex template via aerosol process, Carbon 84 (2015) 281–289.
[35] X.G. Fu, J.Y. Choi, P. Zamani, G.P. Jiang, M.A. Hoque, F.M. Hassan, Z.W. Chen, Co-N decorated hierarchically porous graphene aerogel for efficient oxygen reduction reaction in acid, ACS Appl. Mater. Interfaces 8 (2016) 6488–6495.
[36] W. He, C. Jiang, J. Wang, L. Lu, High-rate oxygen electroreduction over graphitic-N species exposed on 3D hierarchically porous nitrogen-doped carbons, Angew. Chem. Int. Ed. 53 (2014) 9503–9507.
[37] J. Liang, X. Du, C. Gibson, X.W. Du, S.Z. Qiao, N-doped graphene natively grown on hierarchical ordered porous carbon for enhanced oxygen reduction, Adv. Mater. 25 (2013) 6226–6231.
[38] D.Q. Liu, Z. Jia, D.L. Wang, Preparation of hierarchically porous carbon nanosheet composites with graphene conductive scaffolds for supercapacitors: an electrostatic-assistant fabrication strategy, Carbon 100 (2016) 664–677.
[39] G.J. Tao, L.X. Zhang, L.S. Chen, X.Z. Cui, Z.L. Hua, M. Wang, J.C. Wang, Y. Chen, J.L. Shi, N-doped hierarchically macro/mesoporous carbon with excellent electrocatalytic activity and durability for oxygen reduction reaction, Carbon 86 (2015) 108–117.
[40] X. Yu, Y. Kang, H.S. Park, Sulfur and phosphorus co-doping of hierarchically porous graphene aerogels for enhancing supercapacitor performance, Carbon 101 (2016) 49–56.
[41] Y.P. Zhu, Y.L. Liu, Y.P. Liu, T.Z. Ren, G.H. Du, T.H. Chen, Z.Y. Yuan, Heteroatom-doped hierarchical porous carbons as high-performance metal-free oxygen reduction electrocatalysts, J. Mater. Chem. A 3 (2015) 11725–11729.
[42] K. Wan, Z.P. Yu, Z.X. Liang, Polyaniline-derived ordered mesoporous carbon as an efficient electrocatalyst for oxygen reduction reaction, Catalysts 5 (2015) 1034–1045.
[43] G.F. Long, K. Wan, M.Y. Liu, X.H. Li, Z.X. Liang, J.H. Piao, Effect of pyrolysis conditions on nitrogen-doped ordered mesoporous carbon electrocatalysts, Chin. J. Catal. 36 (2015) 1197–1204.
[44] K. Wan, M.Y. Liu, Z.P. Yu, Z.X. Liang, Q.B. Liu, J.H. Piao, Y.Y. Zheng, Synthesis of nitrogen-doped ordered mesoporous carbon electrocatalyst: Nanoconfinement effect in SBA-15 template, Int. J. Hydrog. Energy 41 (2016) 18027–18032.
[45] D. Zhao, J. Feng, Q. Huo, N. Melosh, G.H. Fredrickson, B.F. Chmelka, G.D. Stucky, Triblock copolymer syntheses of mesoporous silica with periodic 50–300 angstrom pores, Science 279 (1998) 548–552.
[46] B. Tian, X. Lui, C. Yu, F. Gao, Q. Luo, S. Xie, B. Tu, D. Zhao, Microwave assisted template removal of siliceous porous materials, Chem. Commun. (2002) 1186–1187.
[47] K. Wan, Z.P. Yu, Q.B. Liu, J.H. Piao, Y.Y. Zheng, Z.X. Liang, An ultrathin 2D semi-ordered mesoporous silica film: co-operative assembly and application, RSC Adv. 6 (2016) 75058–75062.
[48] M. Thommes, K. Kaneko, A.V. Neimark, J.P. Olivier, F. Rodriguez-Reinoso, J. Rouquerol, K.S.W. Sing, Physisorption of gases, with special reference to the evaluation of surface area and pore size distribution (IUPAC Technical Report), Pure Appl. Chem. 87 (2015).
[49] W. Ding, Z. Wei, S. Chen, X. Qi, T. Yang, J. Hu, D. Wang, L.J. Wan, S.F. Alvi, L. Li, Space-confinement-induced synthesis of pyridinic- and pyrrolic-nitrogen-doped graphene for the catalysis of oxygen reduction, Angew. Chem. Int. Ed. 52 (2013) 11755–11759.
[50] S. Chen, J. Bi, Y. Zhao, L. Yang, C. Zhang, Y. Ma, Q. Wu, X. Wang, Z. Hu, Nitrogen-doped carbon nanocages as efficient metal-free electrocatalysts for oxygen reduction reaction, Adv. Mater. 24 (2012) 5593–5597.
[51] Y. Hu, J.O. Jensen, W. Zhang, L.N. Cleemann, W. Xing, N.J. Bjerrum, Q. Li, Hollow spheres of iron carbide nanoparticles encased in graphitic layers as oxygen reduction catalysts, Angew. Chem. Int. Ed. 53 (2014) 3675–3679.
[52] K.F. Blurton, An electrochemical investigation of graphite surfaces, Electrochim. Acta 18 (1973) 869–875.